THE ASTROPHYSICAL JOURNAL, 353:90–102, 1990 April 10

LUMINOSITY-VELOCITY DIAGRAMS FOR VIRGO CLUSTER SPIRALS. I. INNER ROTATION CURVES

DAVID WOODS[1]
Department of Geophysics and Astronomy, University of British Columbia
BARRY F. MADORE[1,2]
Infrared Processing and Analysis Facility, Division of Mathematics, Physics and Astronomy, California Institute of Technology
AND
GREGORY G. FAHLMAN
Department of Geophysics and Astronomy, University of British Columbia
Received 1989 June 28; accepted 1989 October 5

ABSTRACT

Optical rotation curves are presented for the innermost portions of nine spiral galaxies in the Virgo Cluster. The emission-line (Hα and [N II]) velocity data are to be used in combination with new CCD photometry to construct luminosity-velocity diagrams, in a continuing investigation of an apparent initial linear branch and its potential as a distance indicator. Compared to recent H I data, our optical rotation curves generally show systematically steeper inner gradients. We ascribe this effect to the poorer resolution of the H I data and/or to "holes" in the gas distribution. Differences between emission-line and absorption-line rotation curves found, by other workers, for the innermost regions of some spirals, containing significant bulge components, are noted and briefly discussed.

Subject headings: galaxies: clustering — galaxies: internal motions — galaxies: photometry

I. INTRODUCTION

The discovery of a similarity of form in the luminosity-velocity (hereafter L-V) diagrams for a substantial sample of late-type *field* galaxies (Madore and Woods 1987) has prompted us to acquire detailed velocity and photometric data to test this " L-V relation " in the Virgo Cluster. The L-V diagram was first introduced and investigated in an attempt to understand the Tully-Fisher (hereafter T-F) relation (Tully and Fisher 1977) on a more detailed, galaxy-by-galaxy level. In the L-V diagram, the accumulated luminosity (in the form of a magnitude) is plotted versus the logarithm of the local rotational velocity (implicitly as a function of radius) for each galaxy. In this way, an individual spiral galaxy is represented by a detailed growth curve instead of just a single point in L-V space (i.e., an isophotal luminosity and maximum velocity width for the T-F relation). The L-V diagrams, calculated for a sample of 46 field spirals, showed a characteristic initial linear branch (ILB) which were found to have a constant slope (within $\sim 10\%$).

This constancy of the slope of the ILB and its potential as a distance indicator was the motivation for the current Virgo Cluster study. One would like to have L-V diagrams for spiral galaxies in clusters in order to independently determine the dispersion in the slope and especially to find the scatter in the zero point of the ILB. This paper outlines the reduction and analysis of long-slit spectra from which accurate inner rotation curves are produced for nine spiral galaxies in the Virgo Cluster (all of which are within the 6° core, assuming M87 [= NGC 4486] is the center of the cluster).

The number of published rotation curves for spiral galaxies has been growing steadily in recent years, due largely to the efforts of Rubin, her collaborators (Rubin, Ford, and Thonnard 1980; Rubin *et al.* 1982, 1985), and a number of other groups (e.g., Bosma 1981; van Albada *et al.* 1985; Carignan and Freeman 1985). In the past, interest in rotation curves has been concentrated on the internal kinematics of field galaxies. Only recently has a comparison between field and cluster spirals been quantified in terms of their respective rotation curve morphology. In a study of spiral galaxies in the Virgo Cluster and in Abell 1060, Chincarini and de Souza (1985, hereafter CdS) found the rotation curves for cluster galaxies and noncluster glaxies to be quite similar (using optical data), as did Guhathakurta *et al.* (1988, hereafter GvGKB), who have recently obtained H I rotation curves of Virgo spirals. These two studies conflict with the results of Rubin, Whitmore, and Ford (1988) (hereafter RWF), and with Whitmore, Forbes, and Rubin (1988, WFR) who discuss velocity profiles for 21 galaxies in four large, spiral-rich clusters. RWF found significant differences between their field spirals and cluster spirals, including (i) falling rotation curves for inner cluster galaxies, (ii) lower velocity amplitudes for Sa and Sb types, and (iii) a general absence of large, bright, and massive spirals. Since the focus of this study and its subsequent companion papers (Woods *et al.* 1990) is to elucidate the relationship between the cumulative luminosity and the local rotational velocity for the *inner* regions of spirals, the difference between field galaxy rotation curves and the rotation of galaxies in clusters will not be a central issue in our analysis. This is supported by WFR, where no apparent environmental dependence was found for the inner velocity gradient (which is what our data essentially measure), even though a strong correlation is evident between the *outer* velocity gradients and the projected distance of those galaxies from the center of the cluster.

Four galaxies from CdS overlap with our sample. Furthermore, all nine spirals for which we present inner rotation curves have been observed at 21 cm wavelengths, with substan-

[1] Visiting Astronomer, Palomar Observatory.
[2] On research leave from the David Dunlap Observatory, University of Toronto.

tially lower spatial resolution, by GvGKB. We emphasize our need for high–spatial resolution inner rotation curves in order to produce accurate L-V diagrams. Nevertheless, the two aforementioned studies (the CdS paper, in particular) serve as helpful external checks on general morphology and the reproducibility of the rotation curves presented here.

In § II, we discuss how the observations were obtained, and § III describes the subsequent steps required to reduce the data into rotation curves. The analysis of the results of the reduction are presented in § IV, and § V contains a brief discussion, in anticipation of the next paper in this series (Woods *et al.* 1990), which will combine these rotation curve data with newly-obtained surface photometry.

II. OBSERVATIONS

Using the 5 m Hale telescope with the Double Spectrograph mounted at the Cassegrain focus, long-slit spectra of Virgo Cluster galaxies were obtained on the night of 1987 March 15–16. A 1200 lines mm^{-1} grating was centered on the Hα line and imaged on to a TI 800 × 800 CCD detector. The spatial scale was 0".58 per pixel along the slit, and perpendicular to the slit the dispersion was $\sim$0.8 Å per pixel. The slit was opened to a width of 1" in spite of the fact that the seeing was poor throughout the night, varying from 3"–5". Hereafter, we will adopt an average seeing of 4" for the spatial resolution of the spectra. With an adopted distance modulus of 31 mag for Virgo (e.g., Mould, Aaronson, and Huchra 1980), 4" is then equivalent to approximately 300 pc. The length of the slit on the sky is slightly less than 2', and all the spectra had the slit visually centered on the nucleus of the galaxy. The forbidden lines of [N II] ($\lambda\lambda$6548, 6583) and [S II] ($\lambda\lambda$6716, 6731) are commonly observed along with Hα emission, the [N II] λ6583 feature at times being more prominent than the Balmer emission. All the galaxy spectra had exposure times of equal length (2400 s).

Ten Virgo galaxies were observed in total; however, the last object observed, NGC 4647, was dropped from the sample as retained here because of the complex and rather bizarre nature of its resultant rotation curve: NGC 4647 is a member of an interacting pair (Arp 116), and the velocities we obtained from the [N II] and Hα lines radically disagreed with those derived from the [S II] lines. This is perhaps an artifact of the tidal interaction occurring between NGC 4647 and NGC 4649. The velocity field for this intriguing system warrants further, independent study. Another galaxy for which we present an inner rotation curve, but which is clearly too peculiar to consider using for a L-V diagram, is NGC 4388. It has been well established (see § IV) that NGC 4388 is a Seyfert galaxy (the first one discovered in Virgo; Phillips and Malin 1982), and its rotation curve certainly reflects its abnormal status. We will discuss the morphology of its velocity profile in § IV.

III. DATA REDUCTION

The preprocessing (de-biasing and flat fielding) of the spectra was kindly done by Wendy Freedman at the Observatories of the Carnegie Institute of Washington, using reduction programs developed by John Tonry and further modified by Robert Jedzrejewski. Additional reduction and analysis was completed using various IRAF packages and routines (predominantly the *long-slit* package). Each CCD spectrum was corrected for distortion and curvature using (*a*) calibration frames of "holes" (several circular apertures regularly spaced perpendicular to the dispersion axis), taken at the beginning and end of the night, and (*b*) the arc (He-Ne-Ar) exposures, which were obtained after each galaxy spectrum. The arcs have numerous lines with a high signal-to-noise ratio (S/N) in the region surrounding the Hα and [N II] lines but, regrettably, there were not enough arc lines to confidently define the longer wavelength region where the [S II] lines reside. For this reason, we use only the [N II] and Hα lines for our final rotation curves. This is not a tremendous loss, because the [S II] lines are generally weak and appear over a much more limited region of the galaxies studied.

Sky subtraction was performed on all the spectra where it was practical. Since each galaxy completely covered the CCD slit, we could only use the areas where there was no discernible galaxy emission (from any of the lines we were measuring) as the "sky" level to be removed. Three out of nine galaxies in the sample were not sky-subtracted, because there was continuous galaxy emission along the entire length of the slit; these were NGC 4501, NGC 4535 and NGC 4569. To check the effects of sky subtraction on the velocity information, we produced one galaxy's rotation curves with and without sky subtraction (NGC 4192). There was no obvious difference between the two sets of rotation curves at the $\pm$10 km s^{-1} level.

To extract the emission-line positions, we then set up apertures, seven pixel columns in width, across the CCD image. The seven columns of each aperture were then summed to produce one-dimensional spectra, for which the line centroids were measured using the IRAF center-finding algorithm. When there was emission in the outer regions of the galaxy, the apertures were placed side-by-side. In the innermost regions, close to the continuum peak, where there are consistently high S/N emission lines, the apertures were centered on each column. This intensive coverage of the nuclear regions smooths the positional information. It should be emphasized that the points in the innermost regions are *not* independent of each other, as the apertures centered seven pixel columns apart in the outer regions are. We sampled the spectra in this way because it allowed the point of summetry, i.e., the systemic velocity, of each curve to be determined with greater ease.

The internal errors for the velocities, based on the wavelength solution fit, are about $\pm$2 km s^{-1}. The IRAF centering algorithm is most sensitive to the value of the parameter which estimates the width of the emission line(s) being measured. Using a range of emission-line widths, where the width of the emission feature is measured at the continuum level, one can determine the accuracy of the line positions from the repeatability of the results. For each one-dimensional spectrum extracted, the line positions were measured by setting the emission-line width to three pixels for the lower S/N emission in the outer regions and a variety of widths, typically multiples of three pixels, which bracketed the real emission-line width, for the strong emission in the vicinity of the nucleus. Any given line measurement which showed significant disagreement over a reasonable range of emission-line widths was not included in the final rotation curve. There are also parts of some galaxies which do not show spatially continuous emission, due to the discrete nature of the emitting regions, or in some cases the H II regions do not have sufficient S/N to provide accurate information. These two effects introduce breaks in some of the rotation curves presented.

The velocities near the nucleus are better determined, with increasing scatter occurring at larger radii. A conservative estimate of the error for a single measurement of an emission line with a good S/N, i.e., in the vicinity of the nucleus, is about

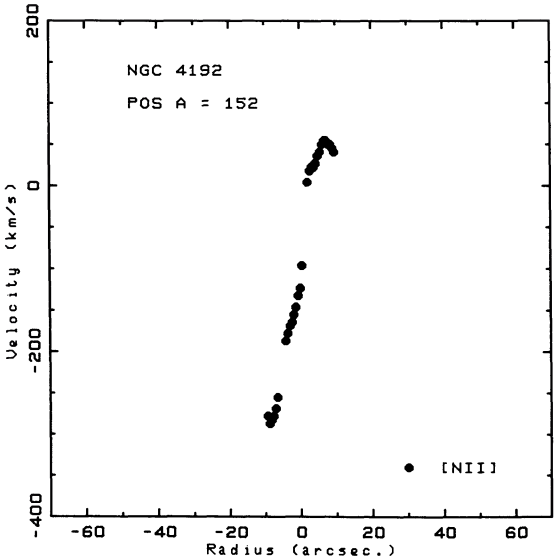

FIG. 1*a*

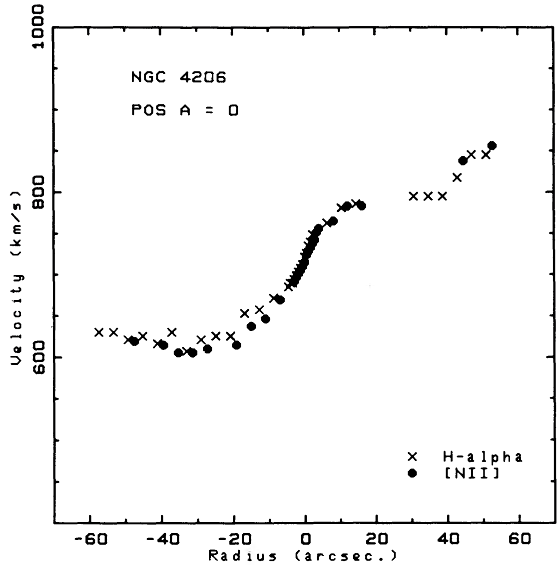

FIG. 1*b*

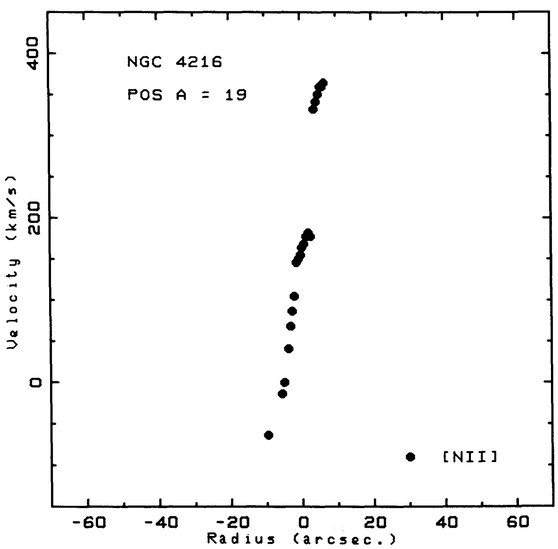

FIG. 1*c*

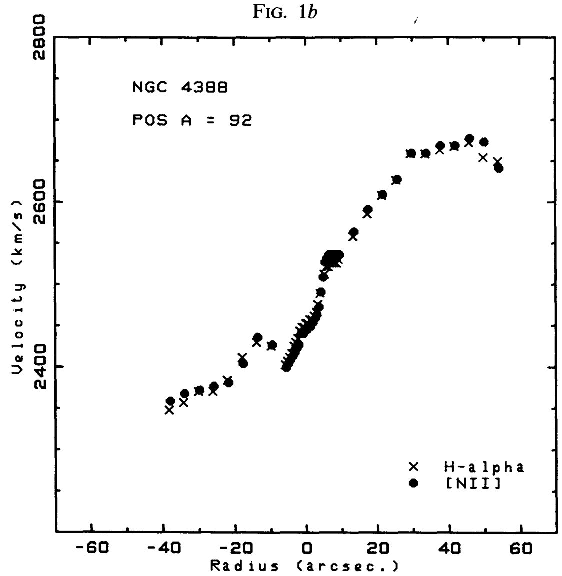

FIG. 1*d*

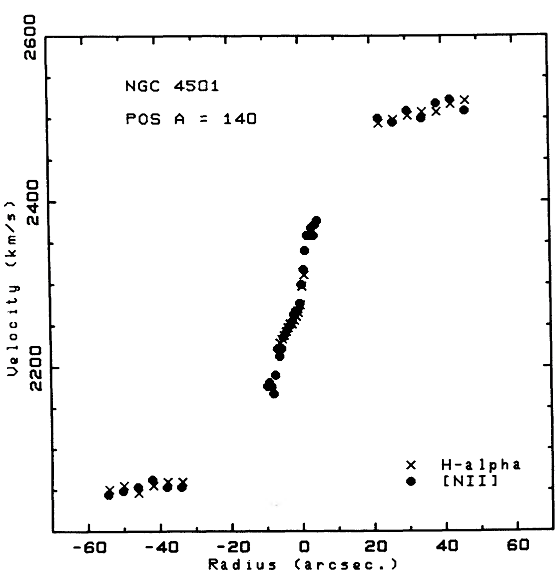

FIG. 1*e*

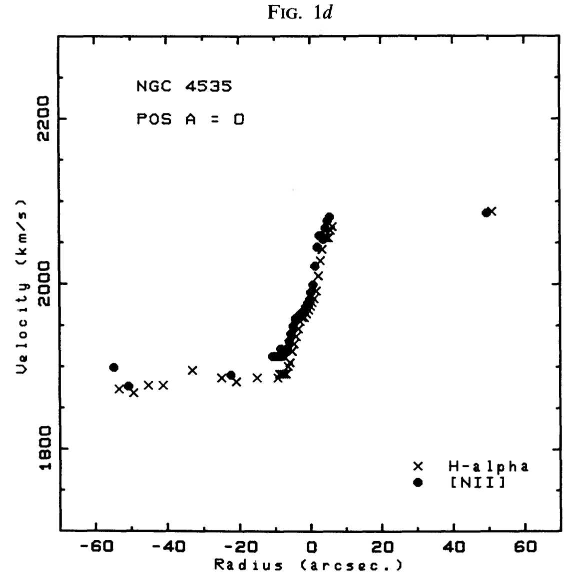

FIG. 1*f*

FIG. 1.—The velocity profiles, before any corrections have been applied to the velocities, and without the reflection about the point of symmetry. Each symmetry point (at zero radius) is that which yields the respective systemic velocity listed in Table 1. Note the good agreement between the Hα velocities (*crosses*) and the [N II] data (*black circles*).

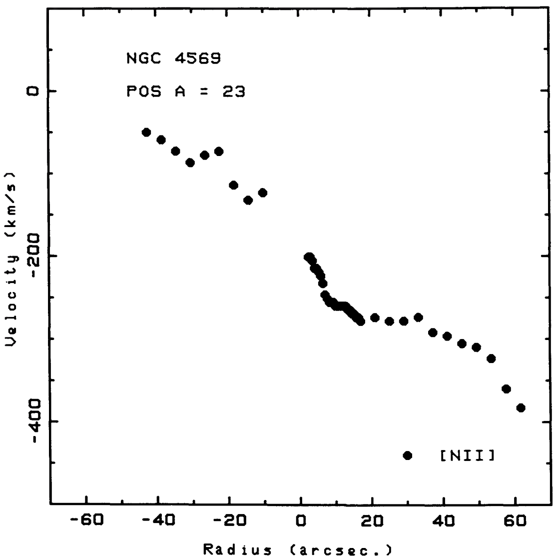

FIG. 1*g*

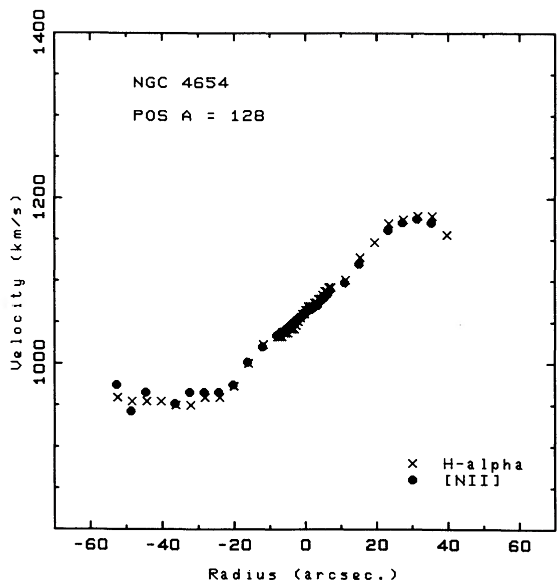

FIG. 1*h*

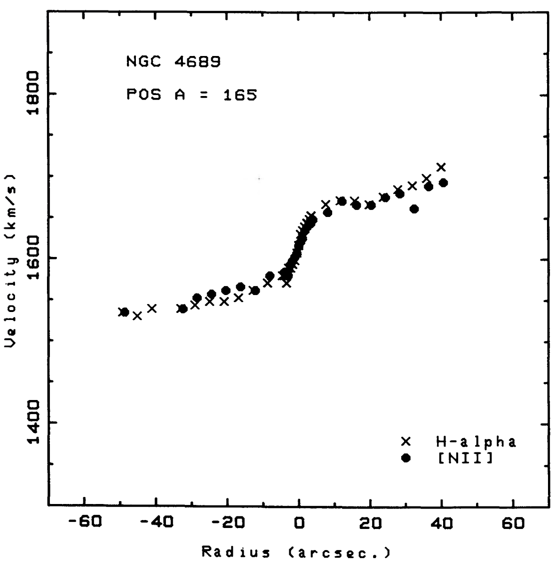

FIG. 1*i*

± 10 km s^{-1}. For data points near the end of the slit, the errors are somewhat higher than this, ± 15–20 km s^{-1}, primarily due to degradation of the S/N. The velocity curves are presented in Figure 1.

Systematic differences between the [N II] and Hα line velocities are present in NGC 4535, NGC 4388 (see also Fig. 2*d*), and possibly NGC 4206. Systematic shifts of this magnitude ($\sim$10–20 km s^{-1}) can also be seen between different lines in some of the rotation curves measured by the Rubin group (e.g., Rubin, Whitmore, and Ford 1988: NGC 2558, WR 66; Rubin *et al.* 1982: NGC 7537, NGC 3054; Rubin *et al.* 1985: IC 724, NGC 3593). We do not understand the origin of this effect. Since our study will focus more on the gradient of the rotation curve rather than the systemic velocity it yields, systematic errors are not as much of a concern as are random errors. There appears to be a slight systematic difference between the gradients found from the [N II] and Hα lines, for NGC 4206, 4654, and 4689.

The systemic velocity for each galaxy was found by iteration: a starting point for the center was chosen, the rotation curve was interpolated to find the systemic velocity, and then the velocities were folded across this position and replotted to see if the resulting rotation curve provided the expected degree of symmetry seen in most spirals. This fitting procedure was continued until a reasonable systemic velocity and symmetric rotation curve were found. The final systemic velocity adopted for each galaxy is a simple average of the systemic velocities determined from the [N II] and Hα rotation curves when both data sets were available.

The final systemic velocities are given in Table 1 ($V_{\odot}$) along with physical data gleaned from other works, and the measured velocity profiles are tabulated in Table 2. Good agreement is found between the systemic velocities in this paper ($V_{\rm opt}$) and those found by GvGKB with H I data. We find a mean difference of $\langle V_{\rm opt} - V_{\rm H\,I} \rangle = 4$ km s^{-1} and a standard deviation from the mean difference of $\sigma_{\langle V_{\rm opt} - V_{\rm H\,I} \rangle} = 28$ km s^{-1}. Comparing our velocities with the Revised Shapley-Ames Catalog (Sandage and Tammann 1981), hereafter (RSA) values yields a higher mean difference: $\langle V_{\rm opt} - V_{\rm RSA} \rangle = 31$ km s^{-1} with a standard deviation $\sigma_{\langle V_{\rm opt} - V_{\rm RSA} \rangle} = 34$ km s^{-1}. Eight galaxies were used for this comparison, because there is no RSA value for NGC 4206.

At this point, the rotational velocities were corrected to edge-on, using the inclinations given by Pierce and Tully (1988). Their inclinations were determined by fitting ellipses to isophotes of the particular galaxy over a range of radii at which the disk dominated the light distribution, from which a characteristic axial ratio was derived. We assume that the rotational velocities we observed are confined to a plane, and that the emitting material is moving in circular orbits. Also, we consider the position angle that each spiral was observed at (see Table 1) to be the true position angle of the major axis. For completeness, the relativistic corrections $1/(1 + z_0)$ (Harrison 1974) were also applied to the velocities, where z_0 is the redshift of each galaxy calculated from its systemic velocity.

The final rotation curves are shown in Figures 2 and 3. The plots in Figure 2 have the GvGKB H I measurements included, where they are shown as asterisks, and the diagrams in Figure

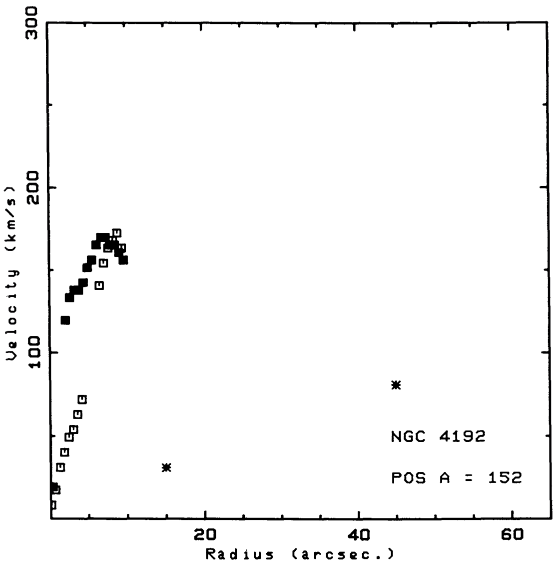

FIG. 2*a*

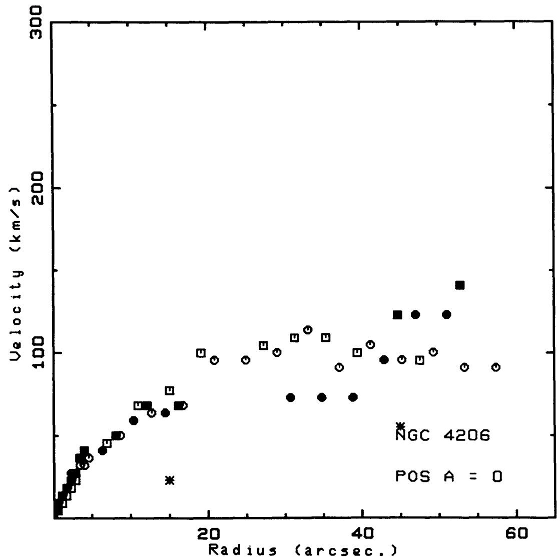

FIG. 2*b*

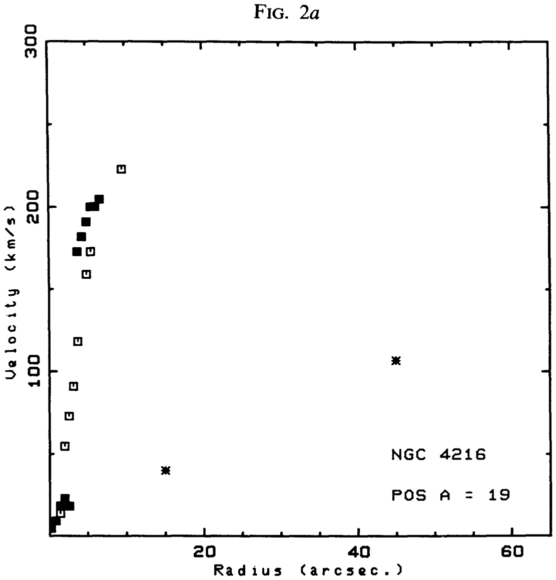

FIG. 2*c*

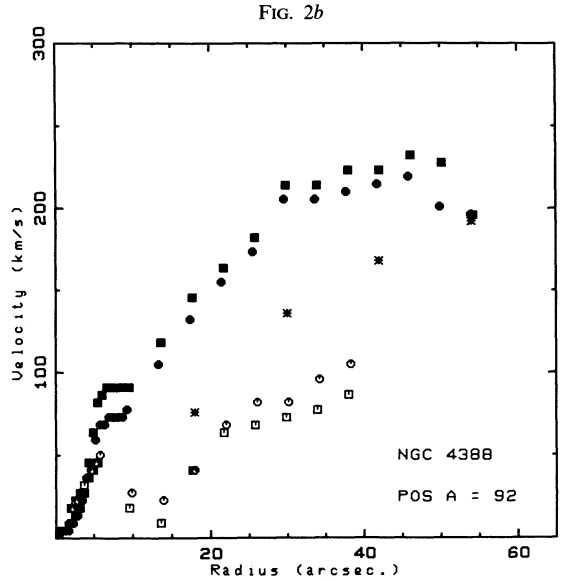

FIG. 2*d*

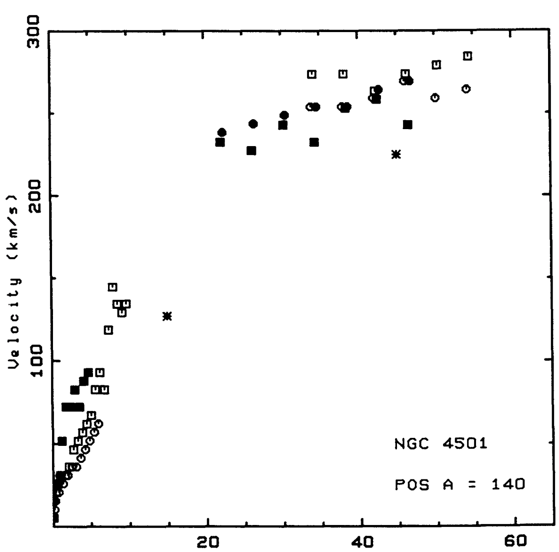

FIG. 2*e*

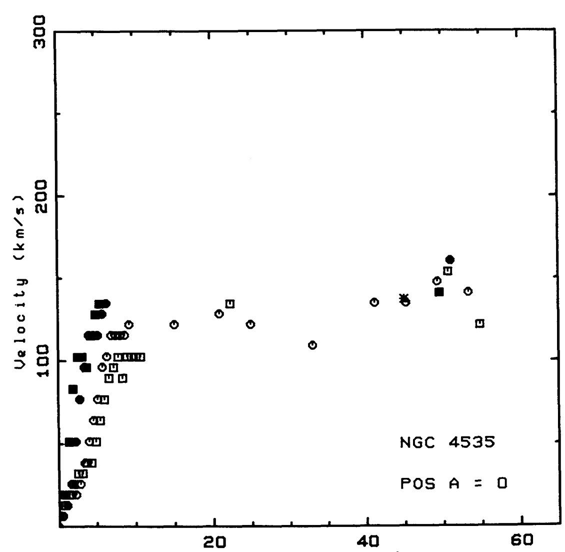

FIG. 2*f*

FIG. 2.—The final rotation curves with the velocities corrected for inclination and relativistic effects. The black and open circles correspond to different sides of the Hα velocity profiles, while the black and open squares are the opposing sides of the [N II] rotation curves. Radio data points gleaned from Guhathakurta *et al.* (1989), uncorrected for our adopted values of the position angle of the major axis and the inclination, are denoted by asterisks.

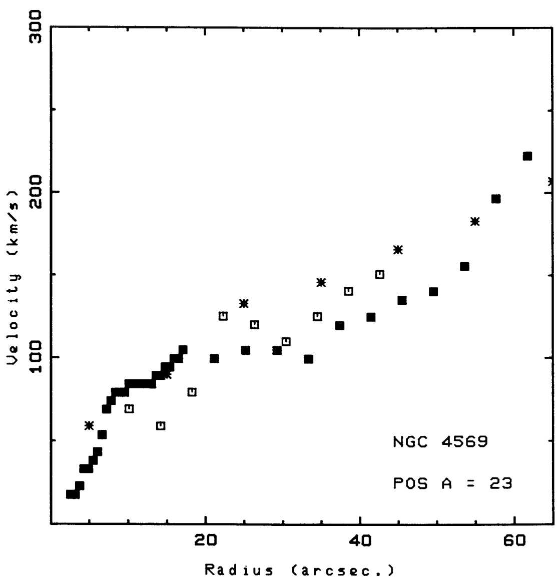

FIG. 2*g*

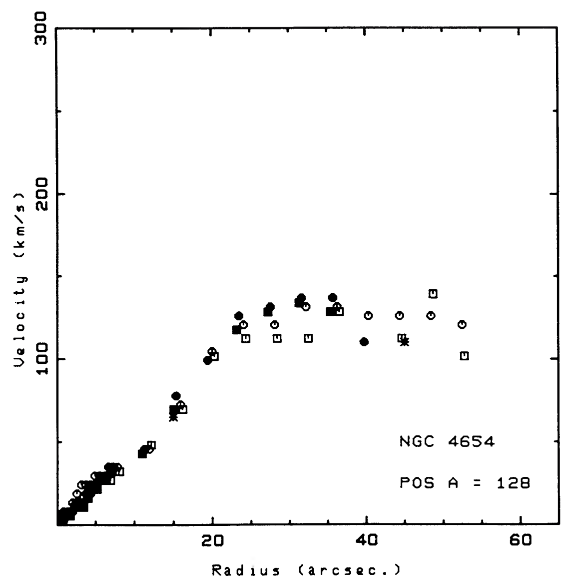

FIG. 2*h*

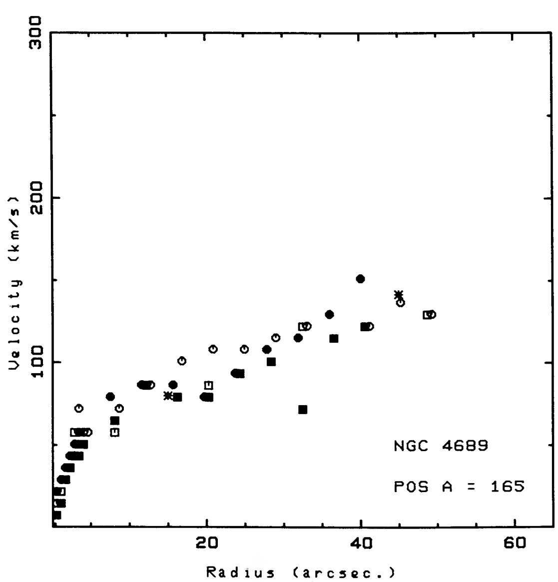

FIG. 2*i*

3 are identical except that the asterisks now correspond to the CdS optical data. Note that the velocities from GvGKB have not been corrected to our adopted inclination and position angle of the major axis for each galaxy, due to these parameters being derived in GvGKB in a multiparameter fit. This could introduce small errors into our comparison of the radio data with our measurements. The CdS data, however, have had these two corrections applied.

IV. ANALYSIS

In this section, we look briefly at the characteristics of the individual rotation curves and how they compare with the H I curves of GvGKB. We also check the consistency between our data and the optical rotation curves from CdS, for the four galaxies in common.

NGC 4192.—This galaxy has emission only in the nuclear and circumnuclear regions. The velocity data from Hα are not included, because this line was partially blended with a night-sky line. A steep velocity gradient is seen, but the gradients on the opposing sides of the nucleus differ considerably. The rotation curve was formed assuming that the slight turnover occurs at the same galactocentric radius in the plane of the galaxy and

TABLE 1

PROPERTIES OF GALAXIES

Galaxy	Type[a] (RSA)	$V_{\odot}$[b] (km s^{-1})	Inclination[c]	Position Angle[d]	B_T[e]	$R_{25}^{i,b}$[f]	Rank[g]
NGC 4192..........	SbII:	−115	86°	152°	10.92	319″	9
NGC 4206..........	Sc(s)	719	90	0	12.79	145	6
NGC 4216..........	Sb(s)	159	90	19	10.97	233	5
NGC 4388..........	Sab	2449	83	92	11.83	162	1
NGC 4501..........	Sbc(s)II	2290	61	140	10.27	223	3
NGC 4535..........	SBc(s)I.3	1979	45	0	10.51	198	7
NGC 4569..........	Sab(s)I–II	−185	63[h]	23	10.23	301	2
NGC 4654..........	SBc(rs)II	1062	58	128	11.14	138	4
NGC 4689..........	Sc(s)II.3	1617	39	165	11.55	120	8

[a] Classification from RSA (Sandage and Tammann 1981).
[b] This work.
[c] Piece and Tully 1988.
[d] Warmels 1988.
[e] RSA.
[f] Whitmore, Forbes, and Rubin 1988.
[g] Guhathakurta *et al.* 1989.
[h] RC2 inclination.

TABLE 2

EMISSION-LINE ROTATION CURVES

Radius (arcsec.)	Velocity (km/s)	Radius (arcsec.)	Velocity (km/s)	Radius (arcsec.)	Velocity (km/s)
		NGC 4192 - [NII]			
-9.5	-278	-1.9	-155	5.1	36
-8.9	-287	-1.3	-146	5.6	41
-8.3	-282	-0.8	-132	6.2	50
-7.7	-278	-0.2	-123	6.8	55
-7.1	-269	0.4	-96	7.4	55
-6.6	-255	2.2	5	8.0	50
-4.2	-187	2.7	18	8.5	50
-3.7	-178	3.3	23	9.1	46
-3.1	-169	3.9	23	9.7	41
-2.5	-164	4.5	27	...	...
		NGC 4206 - $H\alpha$			
-57.4	630	-8.7	672	1.7	740
-53.4	630	-4.6	685	2.3	749
-49.3	621	-4.1	690	6.4	763
-45.2	626	-3.5	690	10.4	781
-41.2	617	-2.9	694	14.5	786
-37.1	630	-2.3	699	30.7	795
-33.1	608	-1.7	704	34.8	795
-29.0	621	-1.2	708	38.9	795
-24.9	626	-0.6	713	42.9	818
-20.9	626	0.0	722	47.0	845
-16.8	653	0.6	726	51.0	845
-12.8	658	1.2	735	...	...
		NGC 4206 - [NII]			
-47.6	619	-2.9	692	2.3	738
-39.4	615	-2.3	697	2.9	742
-35.4	606	-1.7	701	3.5	751
-31.3	606	-1.2	706	4.1	756
-27.3	610	-0.6	710	8.1	765
-19.1	615	0.0	715	12.2	783
-15.1	638	0.6	724	16.2	783
-11.0	647	1.2	729	44.7	838
-7.0	669	1.7	733	52.8	856
		NGC 4216 - [NII]			
-9.6	-64	-1.5	146	2.6	178
-5.5	-14	-0.9	150	3.8	332
-4.9	0	-0.3	155	4.4	342
-3.8	41	0.3	164	4.9	351
-3.2	68	0.9	168	5.5	360
-2.6	87	1.5	178	6.1	360
-2.0	105	2.0	182	6.7	364
		NGC 4388 - $H\alpha$			
-38.3	2348	-1.7	2444	7.5	2526
-34.2	2357	-1.2	2448	8.1	2526
-30.2	2371	-0.6	2448	8.7	2526
-26.1	2371	0.0	2453	9.3	2531
-22.0	2385	0.6	2453	13.3	2558
-18.0	2412	1.2	2458	17.4	2586
-13.9	2430	1.7	2458	21.5	2608
-9.9	2426	2.3	2462	25.5	2627
-5.8	2403	2.9	2467	29.6	2659
-5.2	2407	3.5	2476	33.6	2659
-4.6	2412	4.1	2490	37.7	2663
-4.1	2417	5.2	2512	41.8	2668
-3.5	2426	5.8	2522	45.8	2672
-2.9	2430	6.4	2522	49.9	2654
-2.3	2435	7.0	2526	53.9	2649

TABLE 2—*Continued*

Radius (arcsec.)	Velocity (km/s)	Radius (arcsec.)	Velocity (km/s)	Radius (arcsec.)	Velocity (km/s)
		NGC 4388 - [NII]			
-38.0	2359	-0.9	2441	8.4	2536
-33.9	2368	-0.3	2445	9.0	2536
-29.9	2373	0.3	2445	9.6	2536
-25.8	2377	0.9	2450	13.6	2564
-21.8	2382	1.5	2450	17.7	2591
-17.7	2404	2.0	2454	21.8	2609
-13.6	2436	2.6	2459	25.8	2628
-9.6	2427	3.2	2464	29.9	2659
-5.5	2400	3.8	2473	33.9	2659
-4.9	2404	4.3	2491	38.0	2669
-4.4	2409	4.9	2509	42.0	2669
-3.8	2413	5.5	2527	46.1	2678
-3.2	2418	6.1	2532	50.2	2673
-2.6	2423	6.7	2536	54.2	2641
-2.0	2427	7.3	2536	...	...
-1.5	2441	7.8	2536	...	...
		NGC 4501 - $H\alpha$			
-54.2	2051	-4.3	2243	0.9	2311
-50.1	2056	-3.7	2247	22.4	2494
-46.1	2047	-3.1	2252	26.5	2499
-42.0	2056	-2.6	2252	30.5	2503
-37.9	2060	-2.0	2257	34.6	2508
-33.9	2060	-1.4	2261	38.6	2508
-6.0	2229	-0.8	2266	42.7	2517
-5.5	2234	-0.2	2275	46.8	2522
-4.9	2238	0.4	2298	...	...
		NGC 4501 - [NII]			
-54.4	2045	-5.7	2222	1.9	2359
-50.3	2049	-5.1	2236	2.4	2359
-46.3	2054	-4.5	2240	3.0	2368
-42.2	2063	-3.9	2245	3.6	2359
-38.2	2054	-3.4	2250	4.2	2373
-34.1	2054	-2.8	2254	4.8	2377
-9.7	2177	-2.2	2263	22.2	2500
-9.2	2181	-1.6	2268	26.2	2495
-8.6	2177	-1.0	2268	30.3	2509
-8.0	2168	-0.5	2277	34.3	2500
-7.4	2190	0.1	2300	38.4	2518
-6.8	2222	0.7	2318	42.5	2523
-6.3	2213	1.3	2341	46.5	2509
		NGC 4535 - $H\alpha$			
-53.4	1873	-6.4	1900	1.2	1983
-49.3	1868	-5.8	1905	1.7	1992
-45.2	1878	-5.2	1919	2.3	2010
-41.2	1878	-4.6	1928	2.9	2028
-33.1	1896	-4.1	1937	3.5	2042
-24.9	1887	-3.5	1946	4.1	2056
-20.9	1882	-2.9	1955	4.6	2056
-15.1	1887	-2.3	1960	5.2	2056
-9.3	1887	-1.7	1960	5.8	2065
-8.7	1891	-1.2	1964	6.4	2069
-8.1	1891	-0.6	1969	51.0	2088
-7.5	1891	0.0	1973	...	...
-7.0	1891	0.6	1978	...	...
		NGC 4535 - [NII]			
-54.8	1899	-6.1	1931	0.3	1990
-50.8	1876	-5.5	1940	0.9	1999
-22.3	1890	-4.9	1949	1.5	2022
-10.7	1913	-4.4	1958	2.0	2045

TABLE 2—*Continued*

Radius (arcsec.)	Velocity (km/s)	Radius (arcsec.)	Velocity (km/s)	Radius (arcsec.)	Velocity (km/s)
-10.1	1913	-3.8	1958	2.6	2058
-9.6	1913	-3.2	1963	3.2	2058
-9.0	1913	-2.6	1963	3.8	2054
-8.4	1922	-2.0	1967	4.4	2067
-7.8	1913	-1.5	1972	4.9	2077
-7.3	1917	-0.9	1976	5.5	2081
-6.7	1922	-0.3	1981	49.6	2086
		NGC 4569 - [NII]			
-42.6	-50	6.7	-232	16.0	-273
-38.6	-59	7.3	-246	16.5	-273
-34.5	-73	7.8	-250	17.1	-278
-30.5	-87	8.4	-255	21.2	-273
-26.4	-77	9.0	-255	25.2	-278
-22.3	-73	9.6	-255	29.3	-278
-18.3	-114	10.2	-260	33.4	-273
-14.2	-132	10.7	-260	37.4	-291
-10.2	-123	11.3	-260	41.5	-296
2.6	-200	11.9	-260	45.5	-305
3.2	-200	12.5	-260	49.6	-310
3.8	-205	13.1	-260	53.7	-323
4.4	-214	13.6	-264	57.7	-360
4.9	-214	14.2	-264	61.8	-383
5.5	-219	14.8	-269	...	...
6.1	-223	15.4	-269	...	...
		NGC 4654 - $H\alpha$			
-52.5	959	-4.9	1037	4.4	1078
-48.4	955	-4.4	1042	4.9	1083
-44.4	955	-3.8	1042	5.5	1087
-40.3	955	-3.2	1042	6.1	1087
-36.3	950	-2.6	1046	6.7	1092
-32.2	950	-2.0	1051	7.3	1092
-28.1	959	-1.5	1055	11.3	1101
-24.1	959	-0.9	1060	15.4	1128
-20.0	973	-0.3	1060	19.4	1147
-16.0	1000	0.3	1064	23.5	1169
-11.9	1023	0.9	1069	27.6	1174
-7.8	1032	1.5	1069	31.6	1179
-7.3	1032	2.0	1069	35.7	1179
-6.7	1032	2.6	1074	39.7	1156
-6.1	1037	3.2	1074	...	...
-5.5	1037	3.8	1078	...	...
		NGC 4654 - [NII]			
-52.8	975	-5.2	1043	3.5	1070
-48.7	943	-4.6	1043	4.1	1075
-44.7	965	-4.1	1047	4.6	1079
-36.5	952	-3.5	1047	5.2	1079
-32.5	965	-2.9	1052	5.8	1084
-28.4	965	-2.3	1052	6.4	1084
-24.4	965	-1.7	1056	7.0	1088
-20.3	975	-1.2	1056	11.0	1097
-16.2	1002	-0.6	1061	15.1	1120
-12.2	1020	0.0	1061	23.2	1161
-8.1	1034	0.6	1066	27.3	1170
-7.5	1034	1.2	1066	31.3	1175
-7.0	1038	1.7	1066	35.4	1170
-6.4	1038	2.3	1070	...	...
-5.8	1038	2.9	1070	...	...

TABLE 2—*Continued*

Radius (arcsec.)	Velocity (km/s)	Radius (arcsec.)	Velocity (km/s)	Radius (arcsec.)	Velocity (km/s)
		NGC 4689 - *Hα*			
-49.3	1535	-3.5	1571	3.5	1654
-45.2	1530	-2.9	1590	7.5	1667
-41.2	1539	-2.3	1590	11.6	1672
-33.1	1539	-1.7	1594	15.7	1672
-29.0	1544	-1.2	1599	19.7	1667
-24.9	1549	-0.6	1608	23.8	1676
-20.9	1549	0.0	1617	27.8	1686
-16.8	1553	0.6	1631	31.9	1690
-12.8	1562	1.2	1635	36.0	1699
-8.7	1571	1.7	1640	40.0	1713
-4.6	1581	2.3	1645	...	...
-4.1	1581	2.9	1649	...	...
		NGC 4689 - [NII]			
-48.7	1535	-2.3	1594	4.1	1648
-32.5	1539	-1.7	1598	8.1	1658
-28.4	1553	-1.2	1603	12.2	1671
-24.4	1557	-0.6	1607	16.2	1667
-20.3	1562	0.0	1617	20.3	1667
-16.2	1566	0.6	1621	24.4	1676
-12.2	1562	1.2	1626	28.4	1680
-8.1	1580	1.7	1635	32.5	1662
-4.1	1585	2.3	1639	36.5	1689
-3.5	1585	2.9	1644	40.6	1694
-2.9	1580	3.5	1644	...	...

then using these features to match the amplitudes of the two sides. It can be seen that the resolution of the H I rotation curve (45″) degrades the inner velocity gradient as found in the optical. GvGKB give their first velocity measurement as 31 km s^{-1} at a galactocentric radius of 15″, and their velocities reach $\sim$150 km s^{-1} only starting at 75″. Our data show velocities greater than 150 km s^{-1} within a radius of 10″. In addition to the beam smearing, a deficiency of H I gas in the central area of the galaxy could also contribute to the observed velocity differences. It is possible that the velocity gradients, which we observe, are even steeper, considering the spatial smoothing from our resolution of $\sim$4″. This effect could be most significant for NGC 4192 and 4216 (see Figs. 1*a* and 1*c*), where there are a small number of independent velocity measurements for a compact region near the nucleus.

NGC 4206.—The emission for this highly inclined Sc galaxy is continuous and leads to a well-defined inner rotation curve, with scatter increasing with radius. The H I velocity profile, once again, shows a substantially flatter form due, at least in part, to their lower resolution. Also, GvGKB mention being forced to use the optical center of the galaxy for their fitting procedure, perhaps introducing even more uncertainty for the inner velocities.

NGC 4216.—This rotation curve is reminiscent of NGC 4192. Emission is observed in the nuclear regions only out to a radius of $\sim$10″, although the amplitude of the curve is $\sim$50 km s^{-1} higher than in the case of NGC 4192. Once again, the Hα data were discarded because of blending with a night-sky line. In comparison to our optical data, the H I observations appear to significantly underestimate the amplitude and the gradient of the rotaton curve for the inner regons.

NGC 4388.—Phillips and Malin (1982) were the first to identify this galaxy as a Seyfert. Recently, detailed studies of this galaxy (Pogge 1988; Shields and Filippenko 1988) have suggested that NGC 4388, commonly classified as a Seyfert 2, is an example of a hidden Seyfert 1. The characteristic broad emission lines were very distinctive in many of our central spectra. The velocity profile obtained appears to reflect the peculiar nature of the galaxy, especially the kink in the rotation curve for the approaching side, apparent in Figure 1.

The asymmetry seen in the final rotation curve in Figure 2*d* further demonstrates that this galaxy is peculiar. The strikingly different form of the velocity curve on opposing sides of the major axis has also been seen by GvGKB. For this galaxy, the H I observations had a resolution of 15″ and appear to delineate the velocity gradient with greater success than in other galaxies, but the H I gradient is still substantially shallower than that of our optical data, again possibly due to a lack of H I in the central regions. Surprisingly, the velocity profile presented by CdS shows no evidence of the disparity, seen in our data, in the velocity gradients on opposite sides of the nucleus; and their velocity gradient appears to be comparable to, or even less than, the gradient shown by the H I data.

Systematic differences ($\sim$10 km s^{-1}) between the [N II] and Hα velocities are obviously present in our rotation curve of NGC 4388 but are not large enough to seriously effect the basic form of the profile. Since NGC 4388 is a Seyfert, it will not be included in future L-V diagram analysis. Nevertheless,

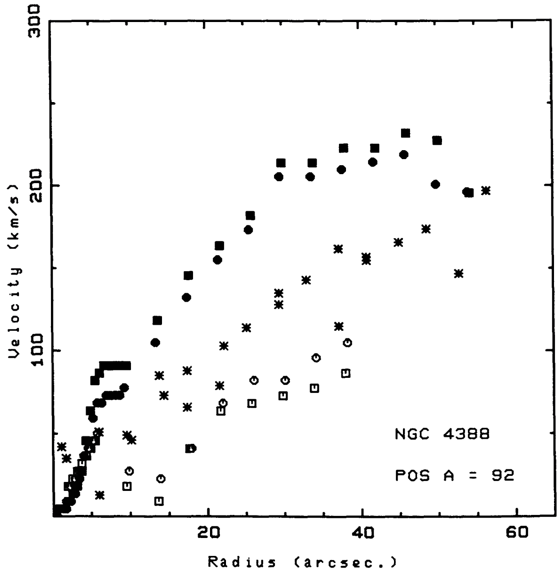

FIG. 3*a*

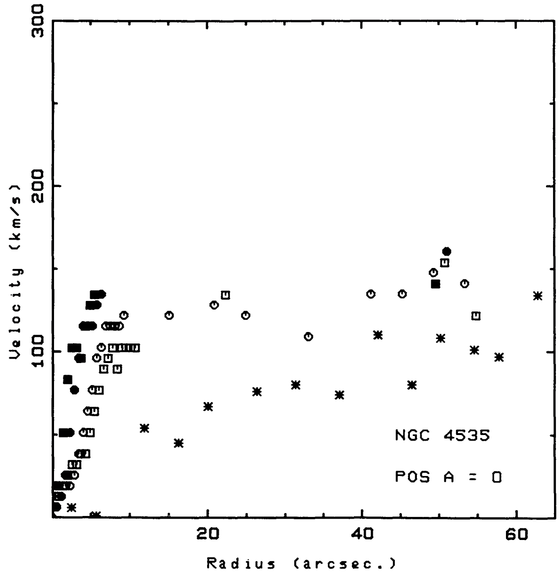

FIG. 3*b*

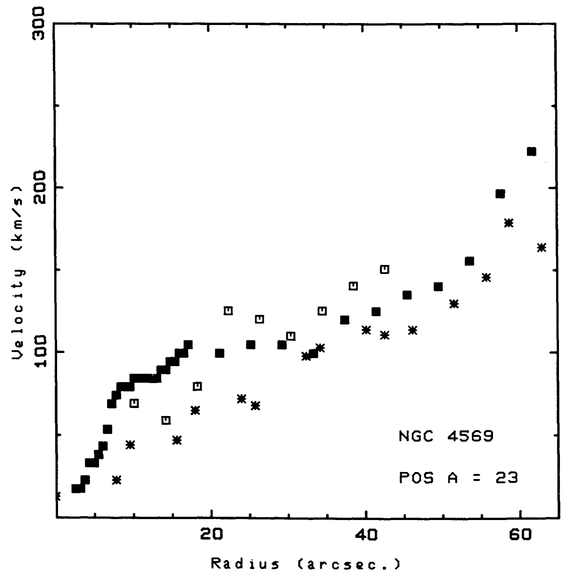

FIG. 3*c*

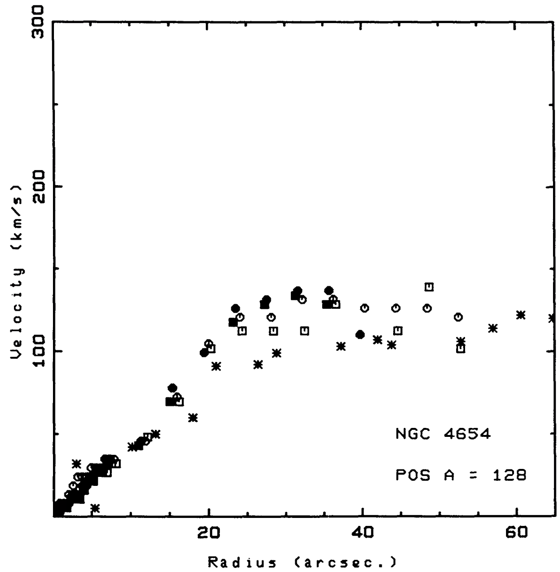

FIG. 3*d*

FIG. 3.—Same as Fig. 2, except the asterisks are the velocities measured at optical wavelengths, as presented in Chincarini and de Souza (1985), corrected for the inclination and position angle of the major axis used in this paper.

this galaxy definitely warrants further study. Velocity-field information from Fabry-Perot interferometry and spectropolarimetric observations would both help establish a better understanding of the mechanism(s) behind this Seyfert's observed properties.

NGC 4501.—The rotation curve, from either the Hα or [N II] lines alone, is well defined. A combination of the data from the two lines, as presented in Figure 2*e*, however, exhibits scatter over the entire profile. The GvGKB H I curve (45″ resolution) is similar to the optical curve at the radii for which H I and optical data are both available. However, the first two data points in the radio curve are still ~25 km s^{-1} lower than our optical velocities.

NGC 4535.—Finding the symmetry point (i.e., the systemic velocity) for this rotation curve was not a simple task, due to the deficiency of velocity data on one side of the nucleus. A fit with considerably less scatter in the inner velocity gradient can be produced, but it yields a velocity profile of peculiar morphology, having very different amplitudes of the velocities on opposite sides of the nucleus. The curve given in Figure 2*f* is a compromise fit. There appears to be a marked difference between the inner velocity gradients for the opposing sides traced by both the Hα and [N II] lines. The H I curve of NGC 4535 overlaps with our optical data at only one point, at a radius of 45″, and the velocity they observe, ~137 km s^{-1}, is in good agreement with our optical value, ~135 km s^{-1}. Optical data presented by CdS show a shallower velocity gradient and an amplitude of the rotation curve which is noticeably lower than ours, scatter in the data being evident over the entire velocity profile.

NGC 4569.—For this galaxy, the Hα data were not used, once again, because of the superposition of a sky line. The

GvGKB H I data, with a resolution of 15″, are in reasonable agreement with the curve in Figure 2*g* but do not appear to resolve the plateau in velocity seen between ~15″–50″ in radius. The CdS velocities indicate that the curve flattens before its final rise around radius 60″.

NGC 4654.—The rotation curve is well defined, with increasing scatter toward the outer regions. The H I data have a slightly shallower gradient but still show good agreement considering the difference in resolution. A substantial difference in the H I kinematics is seen between the velocities measured on different sides beginning at a radius of 75″. Our optical data do not have the spatial extent necessary to check this trend, and the CdS curve shows no evidence of it out to ~1′.5. The CdS rotation curve and our data have very similar velocities.

NGC 4689.—The velocity profile for this galaxy agrees with the sparsely sampled H I rotation curve in GvGKB; neutral hydrogen velocities which overlap with our results are: 80 and 142 km s^{-1} at respective radii of 15″ and 45″. The scarcity of resolved points in the H I data is cited by GvGKB as a cause of the flattening of the velocity gradient.

V. DISCUSSION

A general feature of the above comparisons between the GvGKB H I rotation curves and our optical data is that the inner velocity gradient measured in neutral hydrogen appears to be consistently shallower than the velocity gradient measured by the ionized gas. This effect is most easily explained by the poorer spatial resolution of the radio data, possibly in combination with holes in the neutral gas distribution toward the center of the galaxies in question, which would affect the highly inclined galaxies more strongly. This difference strikingly illustrates the necessity of obtaining high-resolution optical spectra if the rapid rise in rotational motion close to the nucleus is to be accurately determined. Differences between the CdS optical velocities and the rotation curves in this work, e.g., NGC 4388 and NGC 4535, could be a result of CdS using catalog values for their systemic velocities and/or their assumption that the optical center was coincident with the dynamical center.

It is not immediately clear why the CdS and GvGKB data indicate no difference between cluster and field galaxy rotation curves and why RWF and WFR find the opposite result. The approach taken by GvGKB for their comparison between cluster and field galaxies is to superpose the synthetic curves for field spirals of a given morphological type, given by Rubin *et al.* (1985), on the rotation curves for the cluster galaxies. The steeper inner velocity gradients, found here in several cases, should partly explain the discrepancy between the GvGKB results and those of the Rubin group. Also, the approximate nature of the comparison of a specific rotation curve with a mean rotation curve (for several different galaxies of the same morphological type) has the potential to be misleading. The galaxy-by-galaxy gradient analysis adopted by WFR is probably a more physical description of the differences/similarities existing between cluster and field spirals.

In WFR, a good correlation is found between the outer gradient of the rotation curve (defined as the change in velocity from $0.4R_{25}$ to $0.8R_{25}$) and the *projected* distance of the galaxy from the center of the cluster. The inner velocity gradients (measured at $0.15R_{25}$) were tested for a similar relation, with no conclusive result. There are insufficient numbers of galaxies in our sample, with extensive enough spatial coverage, to be able to obtain any kind of meaningful analysis of the *inner* velocity gradients, similar to that presented by WFR. It should be emphasized that the *outer* velocity gradient is used by WFR to conclude that there is a real difference between the rotation curves of field and cluster spirals.

Gradient studies of rotation curves have become fairly common recently. One reason for this may be the close relationship that velocity gradients have with several other global and local physical properties of spiral galaxies. Specifically, Persic and Salucci (1986) have shown that the velocity gradient is directly related to a galaxy's specific angular momentum, kinetic energy and total mass. In another paper, Persic and Salucci (1988) analyze the rotation curves for 43 spirals collected from the literature (very similar to the sample used in Madore and Woods 1987) using gradient analysis. By comparing the logarithmic gradients of the circular velocities predicted by an exponential thin disk model with those observed, they calculate the dark-to-luminous mass ratio within the disk for each galaxy. Baiesi-Pillastrini (1987, 1988) has studied central velocity gradients in spiral galaxies and has found that they correlate with Hubble type, bulge-to-disk ratio, and the pitch angle of spiral arms. This is interpreted as a confirmation that the luminous matter traces the underlying mass distribution in the central regions and that the Hubble classification system succeeds, to some degree, in describing intrinsic properties of galaxies.

Recent detailed observational and modeling work (Fillmore, Boroson, and Dressler 1986, hereafter FBD; Kormendy and Westpfahl 1989, hereafter KW) has suggested that emission-line rotation curves, which follow the gas motions, may not be tracing the true circular motion in the innermost regions of spirals having substantial bulge components. FBD found that constant mass-to-light models could be fit to their observations of six moderately inclined spirals with the three following caveats: (i) there were kinematic differences between the two sides of several of the galaxies, (ii) some of the bulges were flatter than would be expected from their observed rotation rates, and (iii) the emission-line rotation curves fell below the predicted circular velocity for $R \leq 1$ kpc. Absorption-line data were used as the tracer of stars close to the nucleus, and the emission-line data were used to delineate the motion at larger galactocentric distances. KW found a significant difference between the emission-line and absorption-line velocities for the central 35″ of NGC 4594 (the Sombrero galaxy) and also interpreted it as the gas moving at less than the circular velocity.

If emission-line velocities are, in fact, not representative of the true kinematics in the inner regions, this could call into question the interpretation of *some* of the velocities measured in our sample. It should be noted, however, that regardless of what the emission lines are measuring, the correlation seen between the cumulative luminosity and emission-line velocities for the inner parts of spirals in L-V diagrams is an *empirical* relationship, and further observational and dynamical analysis is required to understand its origin. The galaxies most likely to be affected by the difference in emission-line and absorption-line velocities are NGC 4388 and NGC 4569; both are Sab type galaxies, the earliest in our sample. NGC 4192 and NGC 4216, both Sb galaxies, may also be affected to a lesser extent. However, NGC 4388 is a Seyfert and has, in any case, been dropped from the sample. NGC 4569 is one of the galaxies in the FBD sample. The emission-line rotation curves given in FBD are in good agreement with our curve displayed in Figure 2. However, with constant mass-to-light models, FBD show that the expected circular velocity can be obtained in the inner parts only if the kinematics of the bulge, as measured by the absorption-line data, are included in the final fit. This suggests that our observed rotation curve for NGC 4569 is not measuring the true circular velocity.

Perhaps confusing the issue even more is that the original L-V diagram study (Madore and Woods 1987) had a sample of 46 field galaxies which contained roughly an equal number of Sb and Sc types. For all these galaxies, the velocities were determined solely from optical emission lines (Rubin *et al.* 1985). Presumably, the Sb galaxies should have shown an identifiably larger bulge contribution to their kinematics than would the Sc galaxies. If so, it is difficult to understand the constancy of the slope of the initial linear branch (ILB) in the L-V diagrams *if* the emission-line velocities for the Sc types more accurately follow the inner rotation than the similar data for Sb types. The L-V diagram sample was studied for type dependence, and none was found with any confidence; average ILB slopes for the Sb and Sc types were found to differ only at the 1 σ level.

Surface photometry of the Virgo spirals combined with the velocity data in the form of L-V diagrams should help assess the potential of the ILB feature as a distance indicator and, to a lesser extent, help explain the observed kinematical behavior reported here. We defer further discussion until that paper containing surface brightness observations (Woods *et al.* 1990) is published. Also, emission-line and absorption-line rotation curves have been collected for a large sample of Pegasus cluster members. These observations, coupled with surface photometry, should also shed considerable light on the relationship that exists between the distribution of luminous matter and the observed kinematics in spiral galaxies (Woods and Madore 1990). More absorption-line and emission-line rotation curves for late-type galaxies, in clusters, as well as the field, should help to establish over what range of morphological types and scales this difference between absorption-line and emission-line velocities is prevalent. Also requiring further investigation is the environmental dependences for this phenomenon, along with those for velocity gradients and the general morphology of rotation curves.

D. W. would like to dedicate his work on this paper to the memory of Gladys and Ansley Nairn. We would like to thank Wendy Freedman for pre-processing the data and for several useful discussions. D. W. thanks Gerry Grieve for installing the IRAF facility onto the U.B.C. VAX. B. F. M. was supported as part of the *IRAS Extended Mission*, conducted by the Jet Propulsion Laboratory, California Institute of Technology, under contract with NASA. Grants to B. F. M. and G. G. F. from the Natural Sciences and Engineering Research Council of Canada are gratefully acknowledged.

REFERENCES

Baeisi-Pillastrini, G. C. 1987, *Astr. Ap.*, **172**, 375.
———. 1988, *Ap. Letters Comm.*, **27**, 27.
Bosma, A. 1981, *A.J.*, **86**, 1791.
Carignan, C., and Freeman, K. C. 1985, *Ap. J.*, **294**, 494.
Chincarini, G., and de Souza, R. 1985, *Astr. Ap.*, **153**, 218 (CdS).
Filmore, J. A., Boroson, T. A., and Dressler, A. 1986, *Ap. J.*, **302**, 208 (FBD).
Guhathakurta, P., van Gorkom, J. H., Kotanyi, C. G., and Balkowski, C. 1989, *A.J.*, **96**, 851 (GvGKB).
Harrison, E. R. 1974, *Ap. J.* (*Letters*), **191**, L51.
Kormendy, J., and Westpfahl, D. J. 1989, *Ap. J.*, **338**, 752 (KW).
Madore, B. F., and Woods, D. 1987, *Ap. J.* (*Letters*), **323**, L25.
Mould, J., Aaronson, M., and Huchra, J. 1980, *Ap. J.*, **238**, 458.
Persic, M., and Salucci, P. 1986, *M.N.R.A.S.*, **223**, 303.
———. 1988, *M.N.R.A.S.*, **234**, 131.
Phillips, M. M., and Malin, D. F. 1982, *M.N.R.A.S.*, **199**, 905.
Pierce, M. J., and Tully, R. B. 1988, *Ap. J.*, **330**, 579.
Pogge, R. W. 1988, *Ap. J.*, **332**, 702.
Rubin, V. C., Burstein, D., Ford, W. K., Jr., and Thonnard, N. 1985, *Ap. J.*, **289**, 81.
Rubin, V. C., Ford, W. K., Jr., and Thonnard, N. 1980, *Ap. J.*, **238**, 471.
Rubin, V. C., Ford, W. K., Jr., Thonnard, N., and Burstein, D. 1982, *Ap. J.*, **261**, 439.
Rubin, V. C., Whitmore, B. C., and Ford, W. K., Jr. 1988, *Ap. J.*, **333**, 522 (RWF).
Sandage, A., and Tammann, G. A. 1981, *A Revised Shapley-Ames Catalog of Bright Galaxies* (Washington, DC: Carnegie Institution of Washington) (RSA).
Shields, J. C., and Filippenko, A. A. 1988, *Ap. J.* (*Letters*), **332**, L55.
Tully, R. B., and Fisher, J. R. 1977, *Astr. Ap.*, **54**, 661.
van Albada, T. S., Bahcall, J. N., Begeman, K., and Sanscisi, R. 1985, *Ap. J.*, **295**, 305.
Warmels, R. H. 1988, *Astr. Ap. Suppl.*, **72**, 427.
Whitmore, B. C., Forbes, D. A., and Rubin, V. C. 1988, *Ap. J.*, **333**, 542 (WFR).
Woods, D., and Madore, B. F. 1990, in preparation.
Woods, D., Madore, B. F., Fahlman, G. G., and Freedman, W. L. 1990, in preparation.

Note added in proof.—After this paper was submitted for publication, A. S. Wilson kindly pointed out a recent paper by M. R. Corbin, J. A. Baldwin, and A. S. Wilson (*Ap. J.*, **334**, 584 [1988]) which delineates the velocity field of NGC 4388 with greater coverage and accuracy. The [O III] and Hβ velocity field presented in this work confirms the assymmetry we observe in this Seyfert galaxy's rotation curve. Those interested in a more elaborate study of this intriguing galaxy's internal kinematics are directed to the aforementioned paper.

GREGORY G. FAHLMAN and DAVID WOODS: Department of Geophysics and Astronomy, University of British Columbia, Vancouver, BC, Canada V6T 1W5

BARRY F. MADORE: Downs Laboratory 320-47, California Institute of Technology, Pasadena, CA 91125